10th MRIC
8-9th October, 2025
(Multidisciplinary Research International Conference)
University of Wah

Investigating Effectiveness of Encapsulated Phase Change Material Walls for Energy Efficient Buildings

Muhammad Ammar Umar[1], Dr. Muzaffar Ali[2,3], Dr. Muhammad Umar[4], Müslüm Arıcı[2], Tehmina Ambreen[5]

[1] Mechanical Engineering Department, University of Engineering and Technology (UET) Taxila, Taxila 47050, Pakistan. Email: [1]ammarumar@gmail.com

[2] Mechanical Engineering Department, Engineering Faculty, Kocaeli University, 41001 Kocaeli, Turkiye. Email: muzaffar.ali@uettaxila.edu.pk, muslumarici@kocaeli.edu.tr

[3] Department of Energy Engineering, University of Engineering and Technology Taxila, Taxila 47050, Pakistan

[4] Xpert Engineering Solutions, Rawalpindi. Email: muhammadumar@engineer.com

[5] School of Physics, Engineering, and Computer Science, University of Hertfordshire, United Kingdom Email: t.ambreen@herts.ac.uk

Abstract

This study presents a 2D numerical thermal analysis of a test room (1.32 m x 1.32 m) containing a Phase Change Material (PCM) filled capsule in its walls. It contains four walls that are north, south, east, and west walls that are subjected to variable solar heat flux over a 24-hour period. Simulations of two cases are performed, including a conventional wall system and a PCM build-up system. The results show that the PCM system absorbs excess heat during peak solar radiation by melting, as the PCM material has high latent heat, which is the heat absorbed or released during phase change. It can be seen through the results that a significant drop in temperature of the PCM integrated system is observed compared to the simple wall system. The maximum temperature of the room drops by 4.25 K in the encapsulated wall room in comparison with the simple room. The PCM helps to regulate temperature and maintain thermal comfort inside.

Keywords: PCM, Solar Heat Flux, Latent Heat, Solar Radiation, PCM Embedded System, Simple Wall System

1. Introduction

Over the last few decades, worldwide energy consumption has increased enormously, with a 2.2% growth in 2024 alone, fueled by unprecedented weather phenomena and brisk economic growth in the developing world, worsening the exhaustion of fossil fuels that remain the main source of energy despite declining growth rates in oil and coal usage [1]. This escalating demand, projected to continue outpacing efficiency gains through 2050, underscores the urgent need for passive alternative energy sources to reduce reliance on non-renewable resources and mitigate environmental impacts, including rising CO2 emissions [2].

Passive solar building designs, utilizing building location, climate, and materials such as thermal mass (e.g., concrete or phase change materials) to reduce heating and cooling loads by means of strategies such as south-facing windows, overhangs, and natural ventilation, have been shown to achieve significant energy efficiency without mechanical means [3]. Phase change materials (PCMs), which are an integral part of thermal energy storage (TES) systems, have been thoroughly investigated for their capability to absorb and release latent heat, maintaining indoor temperatures and enhancing building thermal comfort; for instance, organic PCMs such as paraffins possess high latent heat capacities (120–280 kJ/kg) and are chemically inert and hence can be incorporated into walls, roofs, and floors [4].

Literature reviews of PCM applications in energy-efficient buildings identify qualitative advantages of lowered temperature fluctuations and improved durability, while quantitative results range from reductions in peak cooling loads by 10–57% and energy cost savings by 10–50% in heating and cooling, varying with seasonal simulations and PCM incorporation techniques such as microencapsulation [5]. Research on encapsulated PCMs in concrete for TES shows up to 50% enhancements in thermal storage capacity, though issues such as a 4.10% reduction in thermal conductivity for each 10% porosity rise and up to 65.8% losses in compressive strength at higher PCM content require optimized methods such as shape-stabilization [6]. Systematic reviews of TES technologies for buildings highlight their applications in waste heat recovery and load shifting, with the efficiency of PCM systems ranging between 75–90% and storage between 50–150 kWh/t, allowing for 10–35% decreases in energy requirements when incorporated into mortars or HVAC systems [7] . Recent developments in PCM for high-temperature building envelopes show temperature declines by 2–7°C and heat gain reductions by 22–62.7%, especially in tropical and Mediterranean climate zones where dual-mode PCMs enhance performance throughout seasons [8].

Research into TES devices in buildings thus far comprises passive integrations such as PCM-enriched gypsum boards with 16.2% cooling demand reduction and active applications where TES is integrated with renewables for 13–17% energy savings over traditional roofs [9]. Bibliometric summaries reflect increasing studies on TES in energy communities, where it provides low-cost alternatives to batteries, although areas remain in climatic adaptability and long-term durability evaluations [10]. Critical reviews highlight PCM design properties, including melting points of

18–40°C for best comfort, resulting in 41% yearly energy savings in Mediterranean climates and 97.1% in ventilated roofs [11] .

Organic PCM application in building materials delivers 11–15% savings in energy for maintaining indoor temperatures at 23°C, where the use of eutectic mixtures delivers narrow phase change ranges for increased sustainability [12]. District heating applications are extended to TES, where water storage of sensible heat delivers 50–90% efficiencies and latent heat through PCMs, allowing volume reduction while achieving 1.4 million GWh/year of savings in Europe [13]. Encapsulated PCM composites, such as capric-myristic acid/vermiculite, have latent heats of 82–147 J/g and provide support for form-stable TES in building envelopes with negligible leakage [14]. Integration of digital twin technology with PCM-TES systems maximizes energy demand, which can cut consumption by 20% by actual-time modeling in smart buildings [15] .

Integrated TES with building components, active and passive systems, enables peak shaving and emissions reductions, sensible storage in concrete packed-beds with efficiencies of 72–96% [16]. Nano-enhanced PCMs further enhance conductivity by 10–20 W/m·K, contributing to 14–79% reductions in energy in cool storage and interior temperature control [17]. Organic PCMs filled with carbon for TES demonstrate thermal conductivity improvement up to 1332%, melting points of 31.5–116°C, and shape-stabilization improvement for applications in buildings [18]. Incorporation of PCMs into wood composites provides latent heats up to 134 J/g and energy savings up to 8.7–41% for cold weather, and stable thermal performance over 200–400 cycles [19]. Overall, PCM-TES developments categorize materials based on phase transition characteristics, with their application to building walls minimizing heat transfer by 47.6% and temperature fluctuations by 46%, demonstrating potential for efficient sustainable energy [20].

2. Materials and Methods

The 2D geometry is a horizontal cross-sectional top view of a simplified model of a room as shown in Figure 1 (a). The outer boundary is represented as a square frame with overall dimensions of 1320 mm by 1320 mm, which covers the building envelope. Beginning from the outside, there is a 5 mm thin layer of plaster for finishing, and then the main structural wall of 150 mm thickness normally equating to concrete or masonry, and an internal 5 mm plaster layer, making the usable inner space a central square of 1000 mm by 1000 mm. For the energy-efficient version illustrated in Figure 1 (c), encapsulated phase change material (PCM) is embedded through a network of hollow cylindrical tubes disposed centrally within the 150 mm wall thickness on four sides; each tube is 936.8 mm long to cover almost the entire wall segment, having an outer diameter of 18.2 mm and a 1 mm wall thickness is show in figure 1 (d) , with the interior hollow space occupied by PCM to absorb and release heat energy during phase transformations, thus moderating the interior temperatures and lowering heating/cooling loads in buildings. Figure 1 (d) shows the dimensions of the plaster, wall, and inside air.

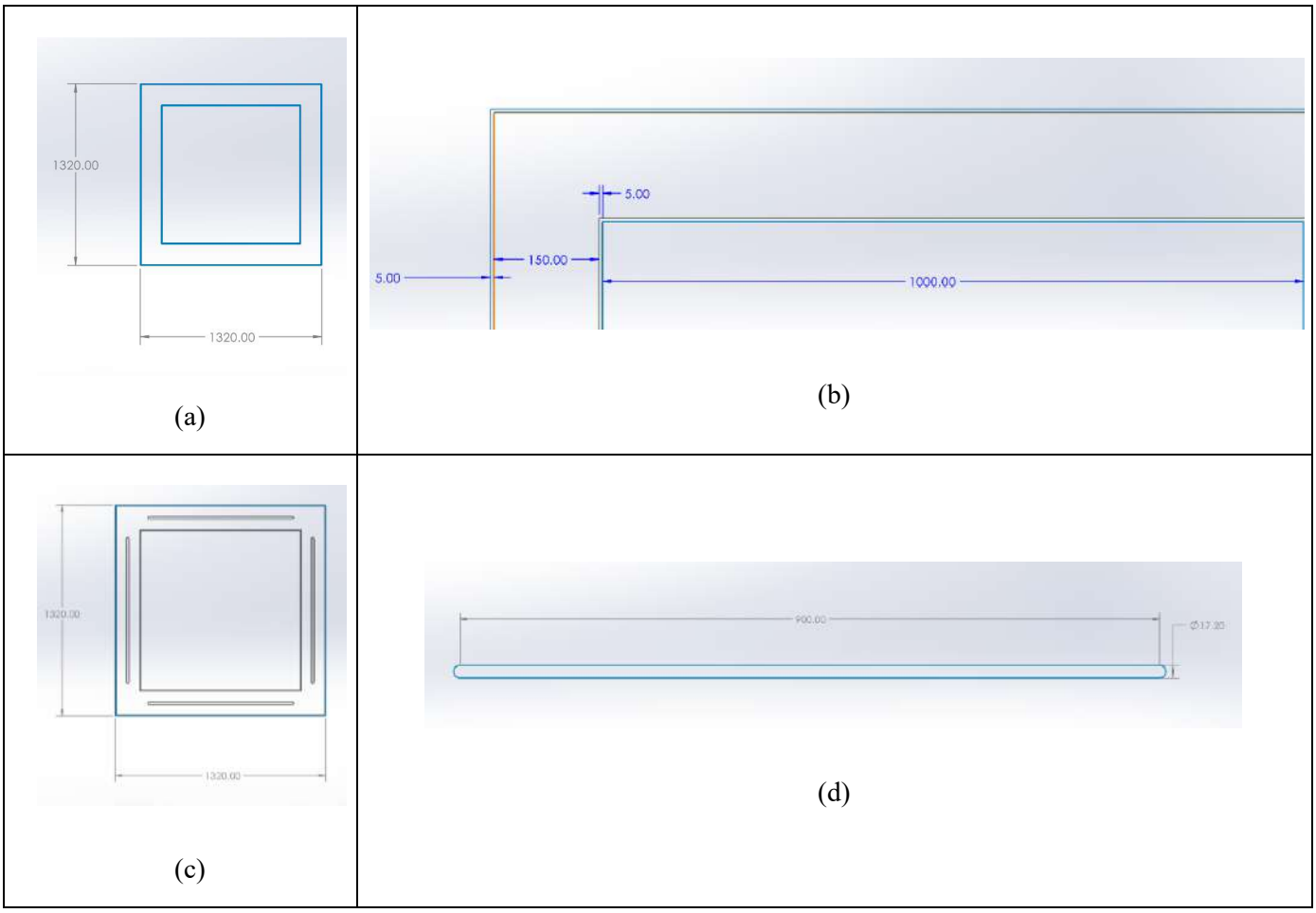

Figure 1: CAD Model of Room Walls Geometry with Dimensions

Table 1 provides the material properties used for the room model, such as air, cement plaster, brick, RT-28-HC (the phase change material), and aluminum (the capsule material). Air, whose low density is 1.22 kg/m³ and specific heat is 1,006.43 J/(kg·K), has low thermal conductivity at 0.0242 W/(m·K) and high viscosity of 1.7894e-05 kg/(m·s), showing it is an insulating medium. Cement plaster, at a density of 1,860 kg/m³ and specific heat of 840 J/(kg·K), has a thermal conductivity of 0.72 W/(m·K), adequate for the outer and inner plaster layers. Brick walls, with a higher density of 1,800 kg/m³ and specific heat of 900 J/(kg·K) and 0.8 W/(m·K) thermal conductivity, supply structural strength. The RT-28-HC PCM has a density of 825 kg/m³, specific heat capacity of 2,000 J/(kg·K), and a high latent heat of fusion of 245,000 J/kg and undergoes a solidus (300 K) to liquidus (302 K) transition temperature, allowing efficient thermal energy storage. Aluminum capsules, with a density of 2,700 kg/m³, specific heat of 900 J/(kg·K), and high thermal conductivity of 220 W/(m·K), hold the PCM inside, facilitating effective heat transfer in the wall system.

Table 1: Properties of Materials

Sr No	Materials	Properties							
		Density ρ (kg/m^3)	**Specific Heat C_p (J/ (kg * K)**	**Thermal Conductivity K (W/ (m *K))**	**Dynamic Viscosity μ (kg/ (m/s)**	**Thermal Expansion Coefficient β (K^{-1})**	**Pure solvent melting heat ΔH_{fus} (J/ kg)**	**Solidus Temperature T_s (K)**	**Liquidus Temperature T_l (K)**
1	Air	1.22	1.006.4	0.0242	1.7894e-05	-	-	-	-
2	Cement Plaster	1860	840	0.72	-	-	-	-	-
3	Brick	1800	900	0.8	-	-	-	-	-
4	PCM (RT-28 HC)	825	2000	0.2	0.005	0	245000	300	302
5	Aluminum	2700	900	220	-	-	-	-	-

3. Mathematical Model

Assuming an incompressible, Newtonian fluid with constant properties (except where phase change affects them), and neglecting viscous dissipation, the key equations are as follows.

3.1 Continuity Equation (Mass Conservation)

The continuity equation ensures mass conservation and, for incompressible flow, takes the form:

$$\frac{\partial \rho}{\partial t} + \frac{\partial (\rho u)}{\partial x} + \frac{\partial (\rho v)}{\partial y} = 0 \qquad (1)$$

Where:

- ρ is the density of the material, which changes during the phase transition.
- t is time (for a transient flow).
- u and v are the velocity components in the x and y directions, respectively.

3.2 Momentum Equations (Momentum Conservation)

The momentum equations are the Navier-Stokes equations modified for phase change. In the enthalpy-porosity approach, a source term $\mathbf{S_m}$ is added to dampen velocities in the solid region, effectively making the solid behave like a porous medium with zero velocity.

$$\rho\left(\frac{\partial \mathbf{u}}{\partial t} + \mathbf{u}\cdot\nabla\mathbf{u}\right) = -\nabla p + \mu\nabla^2\mathbf{u} + \rho\mathbf{g} + \mathbf{S_m} \tag{2}$$

Where:

- ρ is the density,
- t is time,
- p is the pressure,
- μ is the dynamic viscosity,
- $\mathbf{g}$ is the gravitational acceleration vector (e.g., for buoyancy effects if natural convection is involved),
- $\mathbf{S_m}$ is the momentum source term for phase change, defined as:

$$\mathbf{S_m} = -\frac{(1-\beta)^2}{(\beta^3+\epsilon)}A_{\text{mush}}\mathbf{u} \tag{3}$$

Here:

- β is the liquid fraction (0 in solid, 1 in liquid, and between 0 and 1 in the mushy zone),
- ϵ is a small number (e.g., 0.001) to prevent division by zero,
- A_{mush} is the mushy zone constant (typically 10^5 to 10^8 kg/m³·s, user-defined in ANSYS to control the sharpness of the phase transition).

3.3 Energy Equation (Energy Conservation)

The energy equation is formulated in terms of total enthalpy H to handle the latent heat release/absorption during phase change.

$$\frac{\partial(\rho H)}{\partial t} + \nabla\cdot(\rho\mathbf{u}H) = \nabla\cdot(k\nabla T) + S_e \tag{4}$$

Where:

- H is the total enthalpy, expressed as $H = h + \Delta H$,
- $h = \int_{T_{\text{ref}}}^{T} c_p\, dT$ is the sensible enthalpy (with c_p as specific heat capacity),
- $\Delta H = \beta L$ is the latent heat content, where L is the latent heat of fusion,
- k is the thermal conductivity,
- S_e is any additional energy source term (e.g., for heat generation, often 0 in phase change problems).

The liquid fraction β is typically defined as a function of temperature in the mushy zone:

$$\beta = \begin{cases} 0 & \text{if } T < T_{\text{solidus}} \\ 1 & \text{if } T > T_{\text{liquidus}} \\ \dfrac{T - T_{\text{solidus}}}{T_{\text{liquidus}} - T_{\text{solidus}}} & \text{if } T_{\text{solidus}} \leq T \leq T_{\text{liquidus}} \end{cases} \quad (5)$$

Where T_{solidus} and T_{liquidus} are the solidus and liquidus temperatures (equal for pure substances, differing for alloys).

4. Numerical Modelling and Analysis

Figure 2 shows a simple top view of the typical wall system for the room model, consisting of an outer square frame 1320 mm × 1320 mm that surrounds a solid 150 mm thick brick wall. This is clad with 5 mm plaster layers on both inner and outer surfaces, forming a comfortable inner space of 1000 mm × 1000 mm. The wall looks like a broad gray band with thin blue outer shells representing the plaster coverings that clad and finish the building. The enlarged insets are an enlarged view of these thin plaster layers, obviously demonstrating their 5 mm thickness, one inset showing a solid gray area and another showing a dash of blue to clearly demarcate the edge of the layer, presenting a clear and detailed image of the rudimentary wall arrangement utilized in classic building designs.

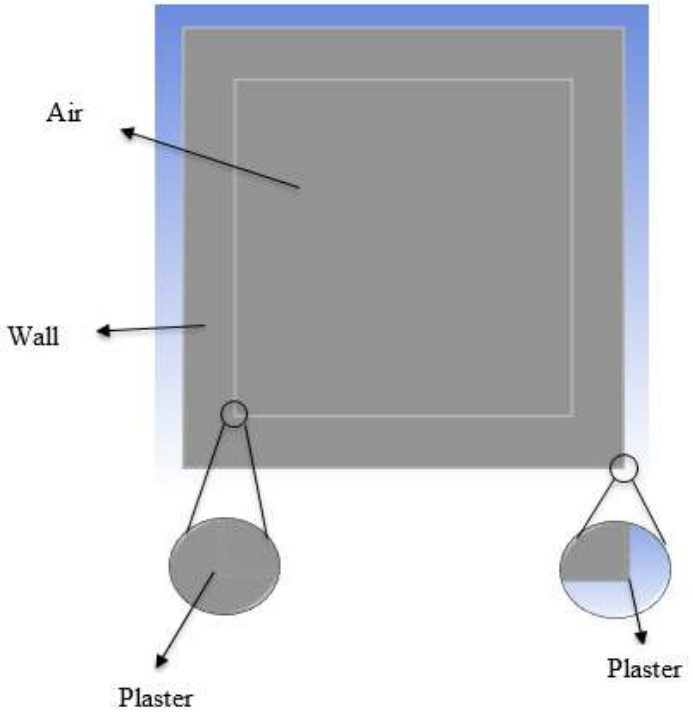

Figure 2: Conventional Wall System Geometry in Design Modeler

The mesh of the traditional wall system is shown in Figure 3, which is a representation of the room model top view with a systematic grid overlay for finite element analysis. The mesh is composed of equal elements of certain sizes: air is meshed in 0.01 m, the outer layer of plaster (Plaster 1) between the outside and the wall is meshed in 0.0025 m, the brick wall is meshed in 0.01 m, and the inner layer of plaster (Plaster 2) between the wall and the inside air is also meshed in 0.0025 m. This configuration has two different layers of plaster; Plaster 1 (external) and Plaster 2 (internal), further improving the accuracy of the model at the interfaces. The mesh is a size mesh with soft behavior with a growth factor of 1.0 that provides a uniform and highly detailed discretization of the 1320 mm × 1320 mm outer frame, 150 mm thick wall, and 1000 mm × 1000 mm inner volume to allow for accurate thermal and structural simulations.

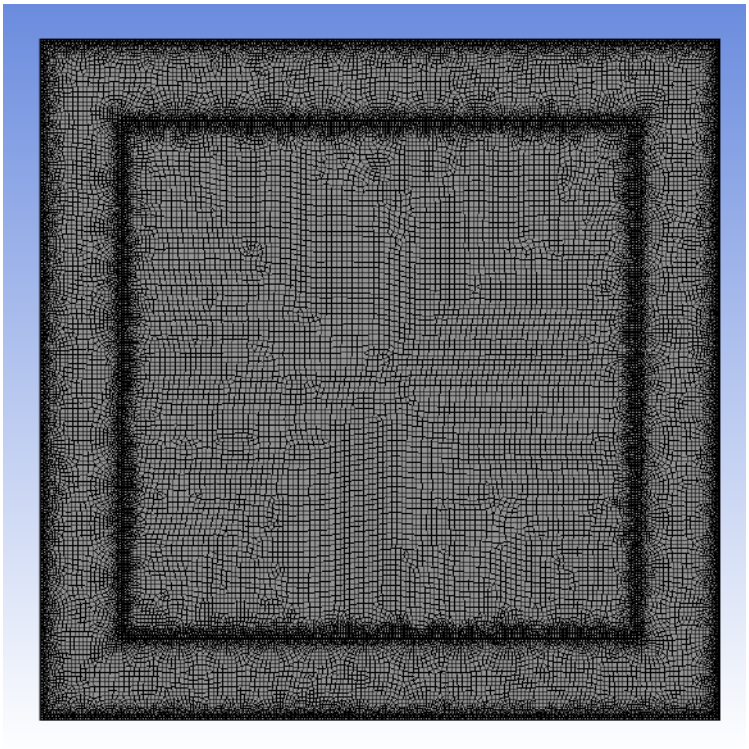

Figure 3: Meshing of Conventional Wall System Geometry

In the setup shown in Figure 4, PCM capsules are centrally placed inside the wall, as illustrated by the enlarged insets: the wall is illustrated in brown, sandwiched between green plaster layers, with the capsules (gray) filled with PCM (blue) placed in the middle. The outer blue layer is the external plaster, while the interior air space is left unaltered, showing how encapsulated PCM improves thermal control inside the original wall structure.

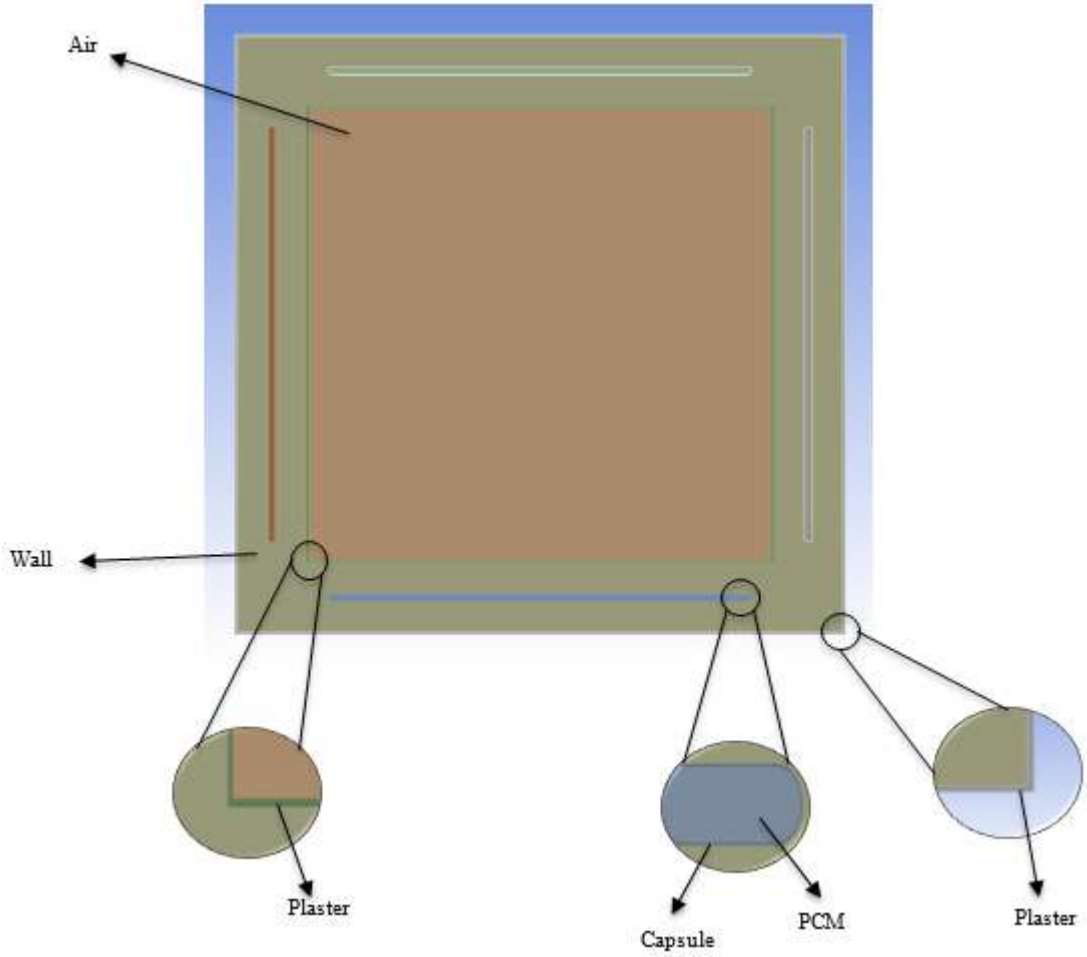

Figure 4: PCM Embedded Wall System Geometry in Design Modeler

Figure 5 illustrates the meshing of the wall system with encapsulated PCM, according to the previous geometry of 1320 mm × 1320 mm outer frame, 150 mm thick brick wall, and 5 mm plaster layers on each side, enclosing a 1000 mm × 1000 mm inner area. The mesh has a structured grid with particular element sizes: air at 0.01 m, Plaster 2 (inner plaster) at 0.0025 m, wall at 0.01 m, capsule at 0.001 m, PCM at 0.00162 m, and Plaster 1 (outer plaster) at 0.0025 m, in the same locations as the traditional case with Plaster 1 exterior to the wall and Plaster 2 interior. This mesh size, with soft behavior and a growth rate of 1.0, provides a consistent and refined discretization, especially near the PCM capsules, for simulating thermal performance in the improved wall structure accurately.

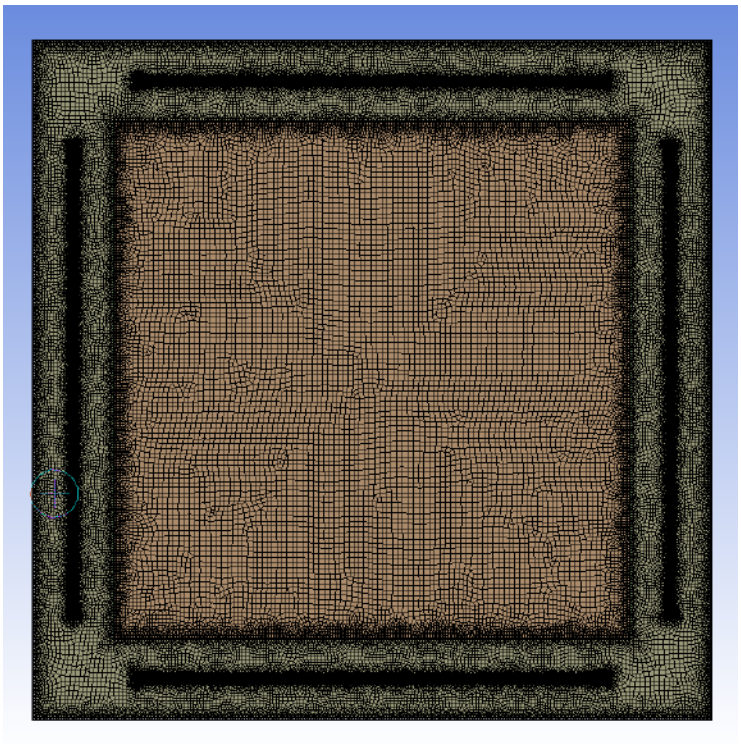

Figure 5: Meshing of PCM Embedded Wall System

5. Problem Set Up

The simulation boundary conditions were based on daily temperature fluctuations for each of the room model walls, with the top defined as north, the right as east, the bottom as south, and the left as west, as shown in Figure 6. The temperatures, in Kelvin, begin at about 299–300 K at 6 AM and increase slowly to highs of 308–323 K between early afternoon and midday before dropping back down to 299–300 K at 6 AM the following morning, illustrating normal daytime solar exposure and ambient conditions affecting the north (coldest, ranging 299–308 K), east (maxing at 323 K), south (maxing at 321 K), and west (maxing at 319 K) walls. Three significant models were utilized in the numerical simulation: the Energy model for the analysis of heat transfer, the Viscous-Laminar model for fluid flow within the air region, and the Solidification/Melting model to simulate the phase change behavior of the RT-28-HC PCM during its phase change from 300 K to 302 K. The transient analysis was simulated for a complete 24 hours, which is equivalent to 86,400 seconds, with a constant time step size of 5 seconds, and a total of 17,280 steps to maximize temporal resolution and accurately capture thermal behavior in the reference conventional wall and PCM-included wall set-ups.

The boundary conditions applied to each wall are shown in Figure 6.

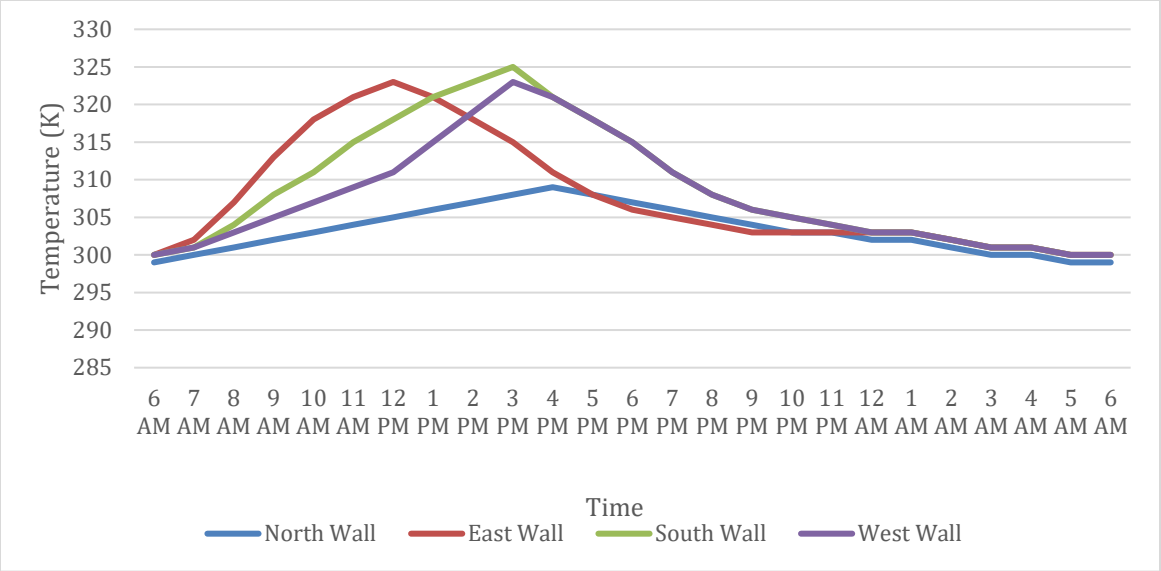

Figure 6: Hourly Fluctuation of temperature on each wall

6. Results and Discussion

The simulation outputs are illustrated by 3-hourly temperature contour plots over 24 hours in Figure 7, identifying differences in thermal performance between the reference wall system and the wall having encapsulated PCM integrated into its thickness, with Table 3 detailing minimum and maximum indoor air temperatures in Kelvin. In the traditional scheme, temperatures begin evenly near 299–300 K at 6 AM (0 hours) and increase smoothly to a maximum of about 325 K at noon (about 9–12 hours, or 9 AM–12 PM), under the diurnal boundary conditions, before falling back to close to initial values after 24 hours, with large gradients from the hotter outer walls towards the center. On the other hand, the PCM-embedded wall has steadier profiles, with top temperatures always lower, reaching only around 310–316 K in the same time interval due to the latent heat of RT-28-HC during its phase transition around 300–302 K, retarding heat penetration. The table measures this effectiveness quantitatively, indicating minimal temperatures reductions (0 K) during early morning when ambient loads are minimal, but increasing benefits during peak heating: a 0.88 K decrease at 12 hours (3 PM), rising to a high of 4.25 K at 15 hours (6 PM), then declining to 3.32 K at 18 hours (9 PM), 1.91 K at 21 hours (12 AM), and 0.85 K at 24 hours (3 AM), proving the PCM's ability to reduce peak indoor temperatures by as much as 1.3% compared to the traditional max, thus improving energy efficiency for building cooling needs without significantly changing minimum temperatures.

Conventional Wall System	Time	Wall with encapsulated PCM
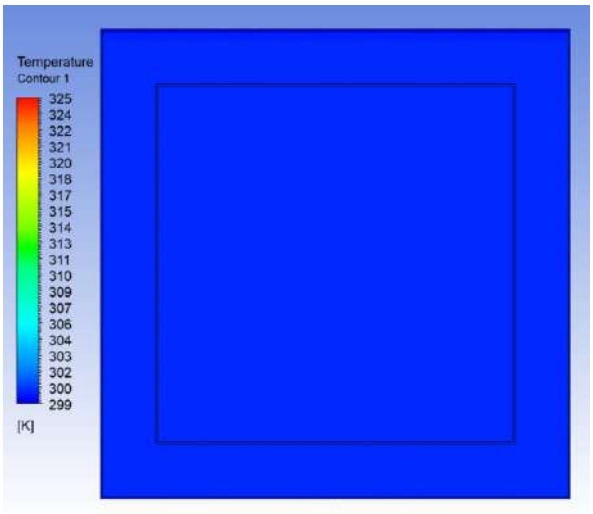	**6AM** **100s** **0 HRS**	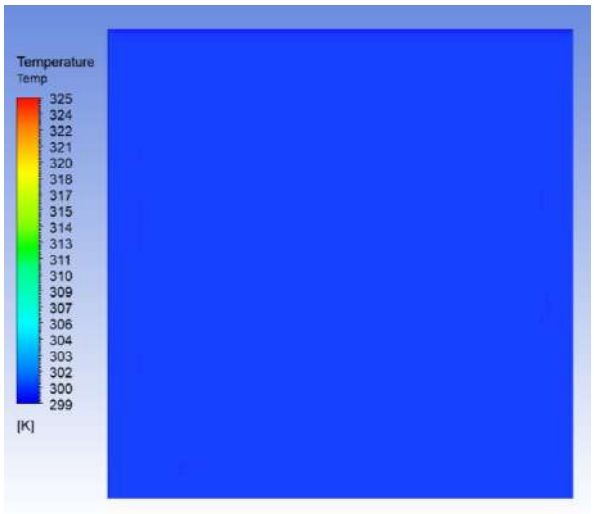
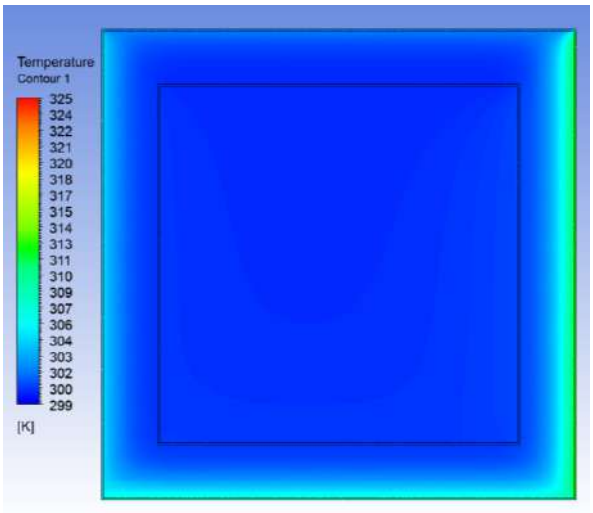	**9AM** **10800s** **3 hrs**	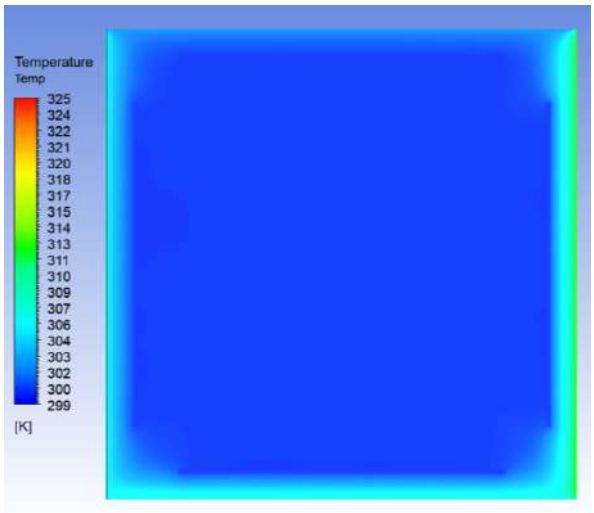
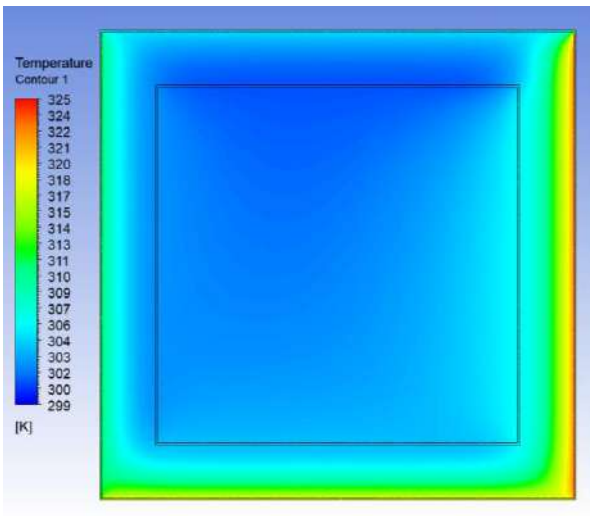	**12PM** **21600s** **6 hrs**	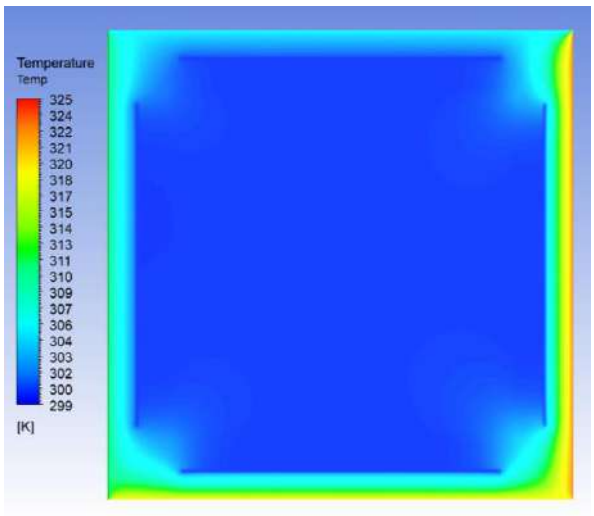

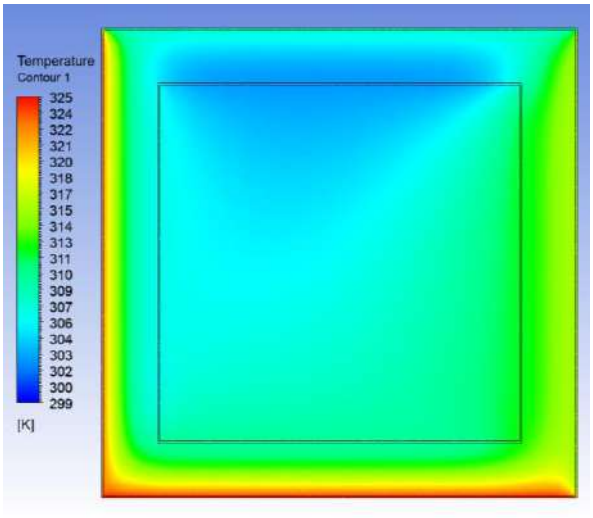	**3 PM** **32400s** **9 hrs**	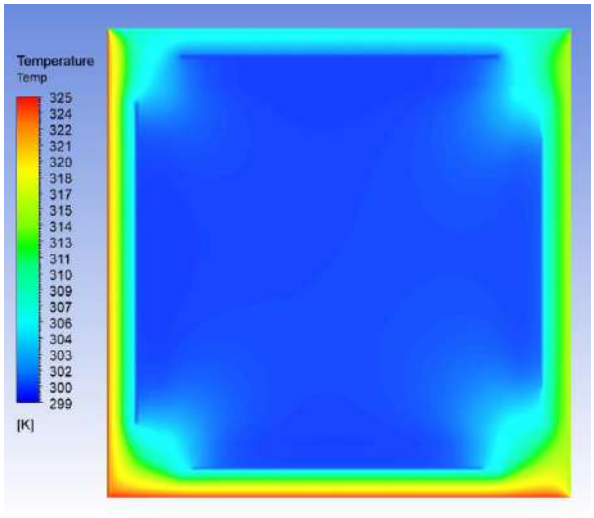
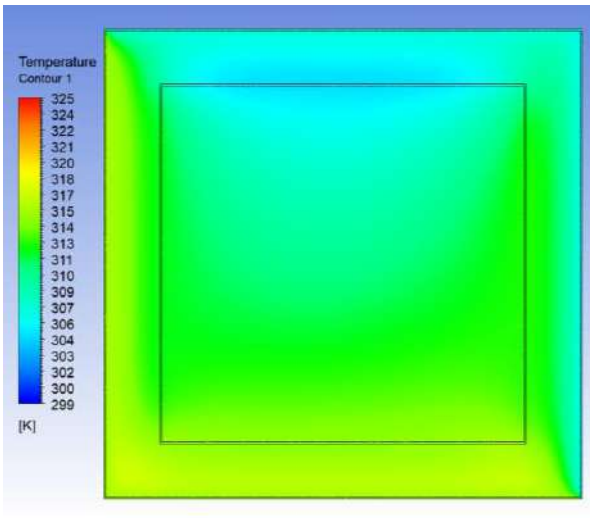	**6PM** **43200s** **12 hrs**	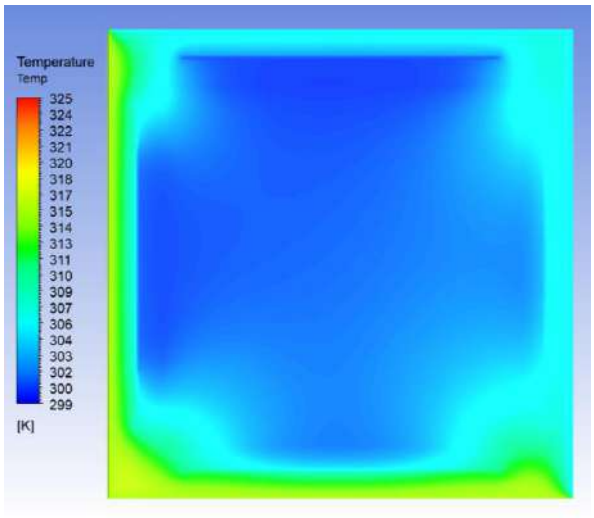
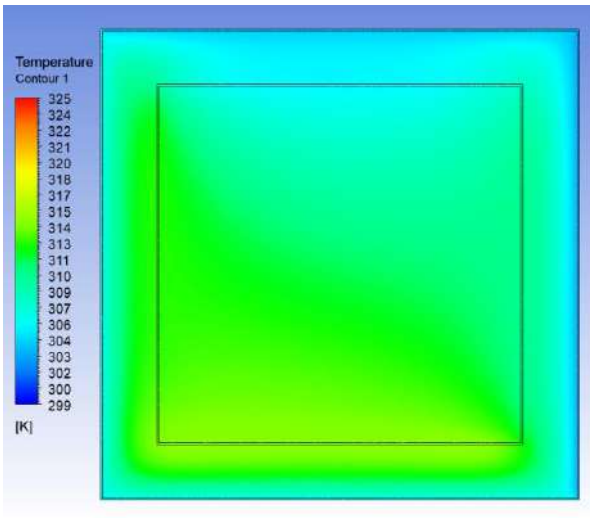	**9PM** **54000s** **15 hrs**	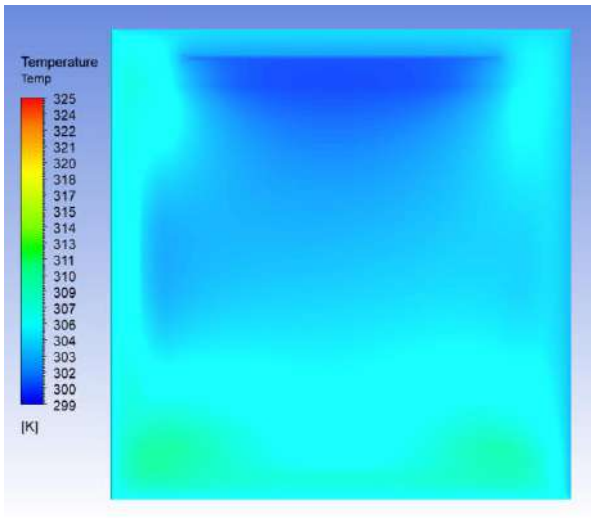

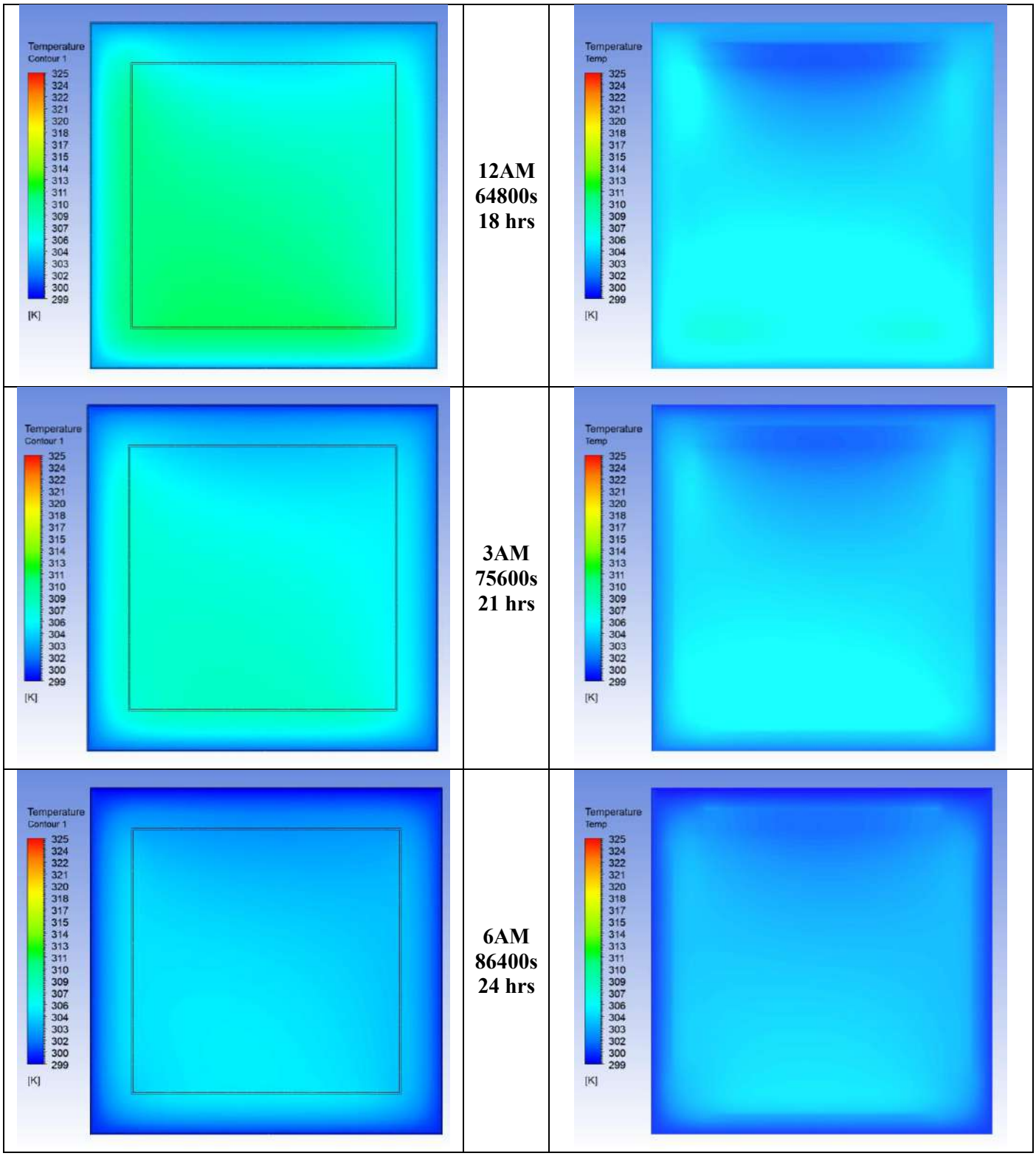

Figure 7: Comparison of Both Cases Contours of Temperature

Table 2: Comparison of Temperature Reduction

Seconds	Hours	Only Walls		Wall with Capsule		Temperature Reduction
		Min temp (K)	Max temp (K)	Min temp (K)	Max temp (K)	
100	0.0278	299.028	300.056	299.028	300.056	0
10800	3	300	313	299.945	313	0
21600	6	300.91	323	299.971	323	0
32400	9	302.663	325	300.002	325	0
43200	12	304.808	316.973	300.114	316.093	0.88
54000	15	303	314.417	300.326	310.167	4.25
64800	18	302	311.053	300.593	307.731	3.322
75600	21	300	307.899	300	305.99	1.909
86400	24	299	305.262	299	304.416	0.846

The CFD results have been compared with experimental work done by Pushpendra Kumar Singh Rathore Et al [21]. Figure 8 shows the variation of temperature (in Kelvin) as a function of time (in hours) for a conventional wall system. The CFD and experimental values of temperature are represented by red and blue lines, respectively. Both curves reveal a diurnal pattern, starting at 302K at t=0h, slowly rising to a peak near 314K near t=12 h, and later declining to 306 K by t= 23 h. The Mean Absolute Error (MAE), which measures the average magnitude of the errors without considering their direction, is 0.47 K. The Root Mean Squared Error, which measures the standard deviation of the residuals, is 0.48 K. Also, the Average Relative Error, which is defined as the absolute differences divided by the experimental values and is indicated as a percentage, is 0.15 %.

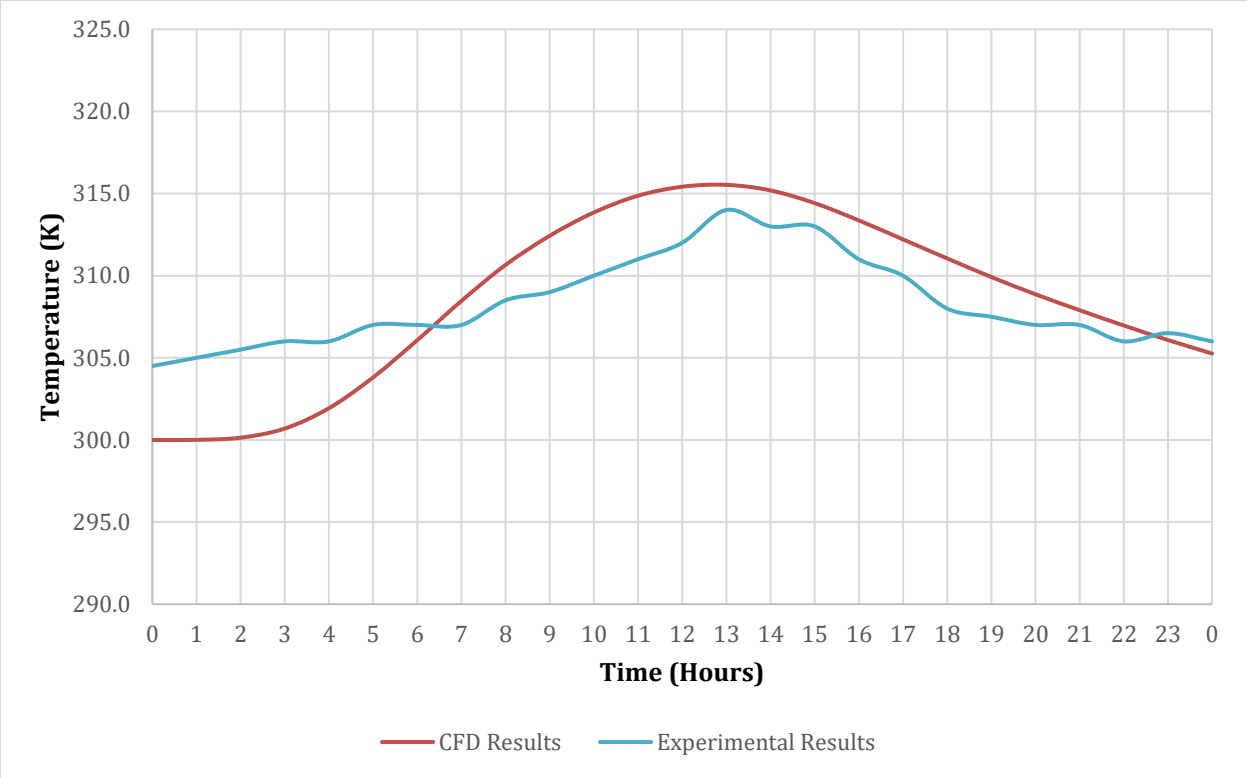

Figure 8: Comparison of inside air temperature through CFD and Experiment (without PCM)

Similarly, Figure 9 compares both results of walls encapsulated with PCM for a period of 24 hours. Both curves follow a diurnal pattern, starting from approximately 303K at t=0 h, rising to up to 310 K near t=14 h due to an increase in thermal load, and then declining to around 306K at t=23h. By performing quantitative analysis, which backs the model's accuracy, the Mean Absolute Error (MAE) is 0.39, the Root Mean Square Error (RMSE) is 0.45K, the relative error averages 0.13%, with a maximum of 0.25% at the peak; these values highlight simulation accuracy within 1% of the measured values. These metrics validate the CFD model's effectiveness in getting the thermal behavior of PCM.

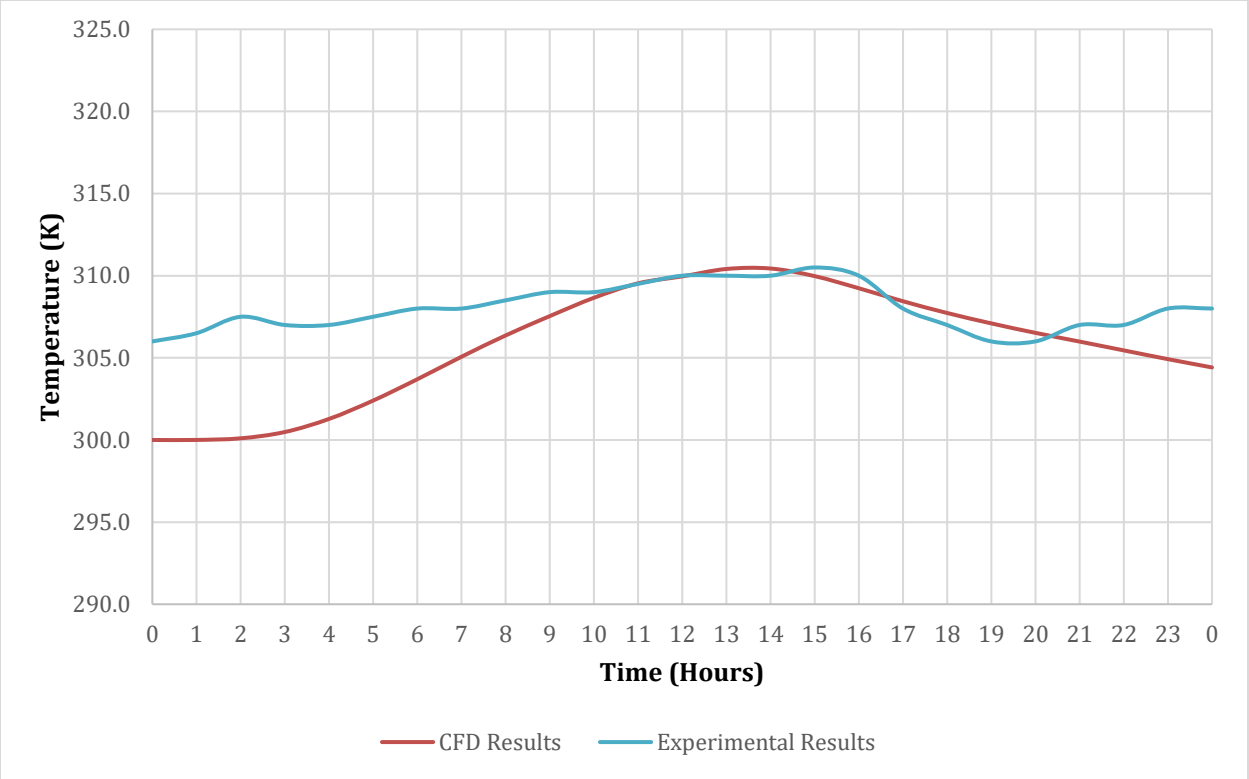

Figure 9: Comparison of inside air temperature through CFD and Experiment (with PCM)

7. Conclusion

After comparing both cases, it is evident that with the use of PCM Rubitherm-28-HC in the walls, the temperature of the room decreases in comparison with the conventional walls case. After simulating for 24 hours for both the cases it is observed that the maximum temperature drop occurs after 15 hours that is 4.25 K. It has been seen that the minimum temperature of the room for every 3 hours in case of wall with capsules has decrease up to 4.69 K. Temperature difference of 3-4 °C or K is significant for maintaining thermal comfort and the PCM capsule in the walls block the heat from ambient to reach inside the room. An initial techno-economic analysis suggests that in environments with diurnal temperature changes, PCM walls could give in 10-30% energy cost saving; nevertheless, high initial costs for encapsulation materials and integration pose a challenge. Limitations include some assumptions of the simulation model, which are considered as constant, like thermal conductivity, density, and other thermophysical properties, along with the dependency of PCM's fusion temperature on local temperature for its effectiveness. However, there may be some variation in such properties, especially during phase transformation. For future recommendations, it is suggested to work on the capsule material and geometry for a better and efficient PCM-based heat storage system, along with a detailed experimental and techno-economic analysis.

8. References

[1] International Energy Agency, "Global Energy Review 2025," International Energy Agency, 2025.

[2] Resources for the Future, "Global Energy Outlook 2024: Peaks or Plateaus?," Resources for the Future, Washington, D.C., 2024.

[3] U.S. Department of Energy, "Passive Solar Homes; Source: Energy.gov," U.S. Department of Energy, Washington, D.C., 2025.

[4] Yaping Cui, Jingchao Xie, Jiaping Liu, Jianping Wang, Shuqin Chen, "A review on phase change material application in building," *Advances in Mechanical Engineering; City: London,* vol. 9, no. 6, 2017.

[5] Usman Masood, Mahmoud Haggag, Ahmed Hassan, Mohammad Laghari, "A Review of Phase Change Materials as a Heat Storage Medium for Cooling Applications in the Built Environment," *Buildings; City: Basel; Publisher: MDPI,* vol. 13, no. 7, p. 1595, 2023.

[6] Authors: Segun Jonathan Osibodu, A. M. Adeyinka, O. V. Mbelu, "Phase change material integration in concrete for thermal energy storage: techniques and applications in sustainable building," *Sustainable Energy Research,* vol. 11, p. 45, 2024.

[7] Authors: Ioan Sarbu, Calin Sebarchievici, " A Comprehensive Review of Thermal Energy Storage," *Sustainability,* vol. 10, no. 1, p. 191, 2018.

[8] Farhan Lafta Rashid, Anmar Dulaimi, Wadhah Amer Hatem, Mudhar A. Al-Obaidi, Arman Ameen, Muhammad Asmail Eleiwi, Sarah Abbas Jawad, Luís Filipe Almeida Bernardo, Jong Wan Hu, "Recent Advances and Developments in Phase Change Materials in High-Temperature Building Envelopes: A Review of Solutions and Challenges," *Buildings; City: Basel,* vol. 14, no. 6, p. 1582, 2024.

[9] Mohammad Saffari, Alvaro de Gracia, A. Fernández, M. Belusko, L.F. Cabeza, "Optimized demand side management (DSM) of peak and off-peak hours using thermal energy storage (PCM) in building applications," *Journal of Cleaner Production,* vol. 171, pp. 378-390, 2018.

[10] Luca Brunelli, Emiliano Borri, Anna Laura Pisello, Andrea Nicolini, Carles Mateu, Luisa F. Cabeza, "Thermal Energy Storage in Energy Communities: A Perspective Overview through

a Bibliometric Analysis," *Sustainability; City: Basel; Publisher: MDPI,* vol. 16, no. 14, p. 5895, 2024.

[11] Xiaonan Wang, Wengui Li, Zhiyu Luo, Kejin Wang, Surendra P. Shah, " A critical review on phase change materials (PCM) for sustainable and energy efficient building: Design, characteristic, performance and application," *Energy and Buildings,* vol. 260, 2022.

[12] Authors: Dhivya Kamaraj, Sellamuthu Ramachandran Rajagopal Senthilkumar, Malathy Ramalingam, Ramkumar Vanaraj, Seong-Cheol Kim, Mayakrishnan Prabakaran, Ick-Soo Kim, "A Review on the Effective Utilization of Organic Phase Change Materials for Energy Efficiency in Buildings," *Sustainability,* vol. 16, no. 21, 2024.

[13] Santosh Chavan, Ramesh Rudrapati, Selvaraj Manickam, "A comprehensive review on current advances of thermal energy storage and its applications," *Alexandria Engineering Journal,* vol. 62, pp. 83-100, 2022.

[14] " Thermal Energy Storage by the Encapsulation of Phase Change Materials in Building Elements—A Review," *Materials; City: Basel; Publisher: MDPI,* vol. 14, no. 8, p. 2010, 2021.

[15] Mohammad Waseem, Mumtaz Ahmad, G. Sree Lakshmi, Areti M.S.V. Sushma, Sanjay Paul, Mohammad Afaza, "Role of phase change materials and digital twin technology in thermal energy storage system: A review," *International Journal of AI for Materials and Design; City: Singapore,* vol. 1, no. 3, p. 50–65, 2024.

[16] Johan Heier, Chris Bales, Viktoria Martin, "Combining thermal energy storage with buildings - A review," *Renewable and Sustainable Energy Reviews,* vol. 42, pp. 659-675, 2015.

[17] Javad Mohammadpour. Ann Lee, Victoria Timchenko, Robert Taylor, "Nano-Enhanced Phase Change Materials for Thermal Energy Storage: A Bibliometric Analysis," *Journal of Energy Storage,* vol. 63, 2022.

[18] Guijun Yang, Yoon-Ji Yim, Ji Won Lee, Young-Jung Heo, Soo-Jin Park, "Carbon-Filled Organic Phase-Change Materials for Thermal Energy Storage: A Review," *Molecules,* vol. 24, no. 11, 2019.

[19] Authors: G. E. Rodríguez, C. Bustos Ávila, A. Cloutier, "Use of phase change materials in wood and wood-based composites for thermal energy storage: A Review," *BioResources,* vol. 18, no. 4, 2023.

[20] Christina V. Podara, Ioannis A. Kartsonakis, Costas A. Charitidis, "Towards Phase Change Materials for Thermal Energy Storage: Classification, Improvements and Applications in the Building Sector," *Applied Sciences,* vol. 11, no. 4, 2021.

[21] Pushpendra Kumar Singh Rathore, Shailendra Kumar Shukla, "An experimental evaluation of thermal behavior of the building envelope using macroencapsulated PCM for energy savings," *Renewable Energy,* vol. 149, pp. 1300-1313, 2020.